Stepwise conversion of a *single source precursor* into crystalline AlN by transamination reaction

Stephan Schulz[a,*], Tillmann Bauer[b], Wilfried Hoffbauer[b], Jörn Schmedt auf der Günne[c], Markus Doerr[d], Christel M. Marian[d], Wilfried Assenmacher[e]

[a]*Institute of Inorganic Chemistry, University of Duisburg-Essen, Universitätsstrasse 5-7, 45141 Essen, Germany*
[b]*Institute of Inorganic Chemistry, University of Bonn, Gerhard-Domagk-Str. 1, 53121 Bonn, Germany*
[c]*Department of Chemistry and Biochemistry, University of Munich (LMU), Butenandtstr. 5-13, D2.076, 81377 München, Germany*
[d]*Institute of Theoretical and Computational Chemistry, University of Düsseldorf, Universitätsstr. 1, 40225 Düsseldorf, Germany*
[e]*Institute of Inorganic Chemistry, University of Bonn, Römerstr. 164, 53117 Bonn, Germany*

Abstract

Ammonolysis of the monomeric, base-stabilized trisaminoalane $Me_3N-Al[N(H)Dipp)]_3$ (Dipp = 2,6-$^iPr_2$–C_6H_3) yielded Al–N oligomers, which were characterized in detail by solid state NMR spectroscopy (^1H, ^{13}C, ^{15}N, ^{27}Al) and TGA/DTA. Pyrolysis of as-prepared oligomers at different temperatures in an argon steam yielded carbon-containing black solids, whereas pyrolysis under a steady flow of NH_3 produced pure aluminum nitride (AlN). The role of the pyrolysis temperature and the influence of NH_3 on the formation of crystalline materials were investigated. As-prepared AlN was characterized by solid state NMR spectroscopy (^{15}N, ^{27}Al), X-ray diffraction (XRD), transmission electron microscopy (TEM) and electron energy loss spectroscopy (EELS). Theoretical calculations were performed in order to identify potential reaction intermediates.
© 2007 Elsevier Inc. All rights reserved.

Keywords: Single source precursor; Ammonolysis; AlN; Solid state NMR
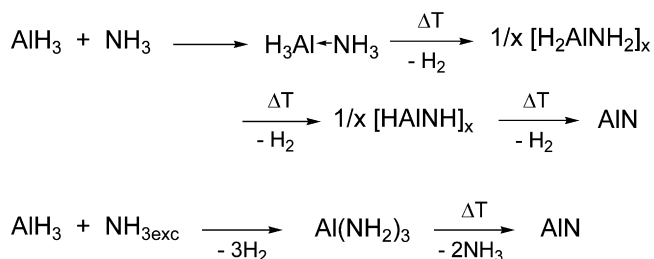
1. Introduction

Aluminum nitride (AlN) is a ceramic material that has received considerable interest in the last decade due to its excellent combination of high thermal conductivity, low thermal expansion coefficient, excellent chemical and thermal stability and good mechanical strength. Thin films are typically obtained from vapor deposition techniques (MOCVD) [1], whereas bulk materials are usually synthesized by high-temperature processes such as direct nitridation of Al metal or Al_2O_3 with N_2 or NH_3 [2], carbothermal reduction/nitridation [3] and SHS processes [4] as well as by reaction of $AlCl_3$ with NH_3 [5] or NaN_3 [6]. An alternative, low-temperature approach to AlN films [7] as

well as bulk AlN uses so-called *single source precursors*, which contain the elements of the desired material (e.g. Al and N) connected by a stable chemical bond [8]. In fact, the very early study of Wiberg et al. [9] more than 60 years ago on the reaction of H_3Al and NH_3 already demonstrated that the formation of bulk AlN proceeds via formation of reaction intermediates such as the Lewis acid-base adduct H_3Al–NH_3, the aminoalane $[H_2AlNH_2]_x$ and iminoalane $[HAlNH]_x$. In addition, the reaction of AlH_3 with an excess of NH_3 yielded $Al(NH_2)_3$ [10], which also was found to be a suitable single source precursor for AlN (Scheme 1).

Unfortunately, the thermal stability of as described compounds, which are ideal single source precursors for the formation of AlN due to the lack of any carbon-containing organic substituents, is rather low. Consequently, kinetically stabilized precursors such as amine-alane adducts R_3Al–NR_3, aluminum amides ($Al[NR_2]_3$, $[R_2AlNR_2]_x$,...)

*Corresponding author. Fax: +49 5251 603423.

E-mail address: stephan.schulz@uni-due.de (S. Schulz).

$$AlH_3 + NH_3 \longrightarrow H_3Al{\leftarrow}NH_3 \xrightarrow[-H_2]{\Delta T} 1/x\,[H_2AlNH_2]_x$$

$$\xrightarrow[-H_2]{\Delta T} 1/x\,[HAlNH]_x \xrightarrow[-H_2]{\Delta T} AlN$$

$$AlH_3 + NH_{3exc} \xrightarrow[-3H_2]{} Al(NH_2)_3 \xrightarrow[-2NH_3]{\Delta T} AlN$$

Scheme 1. Reaction of AlH_3 with NH_3 as reported by Wiberg et al.

and imides $[RAlNR]_x$, which are accessible by standard reactions such as alkane elimination and salt metathesis reactions, were investigated. Transamination reactions were found to produce bulk AlN in a multistep reaction process via formation of oligomeric reaction intermediates, which yield AlN powders under pyrolysis conditions at higher temperatures. For instance, the reaction of $[Al(NMe_2)_3]_2$ and NH_3 initially yielded a mixed Al-amide-imide oligomer $[Al(NH)NH_2]_x$, which still contained NMe_2 groups to some extent [11]. Pyrolysis of this oligomer in an Ar flow resulted in the formation of a black solid material indicating a high level of carbon (due to organic residues), whereas a light gray, nanocrystalline AlN powder was formed in a steam of NH_3 between 900 and 1100 °C. Comparable results were obtained with $[Ga(NMe_2)_3]_2$ [12], which reacts with NH_3 with formation of gallium imide $[Ga(NH)_{3/2}]_2$ and heterocyclic aminogallane $[H_2GaNH_2]_3$ [13]. Both precursors were pyrolyzed under a flow of Ar or NH_3 at 500 and 600 °C, respectively, yielding mixtures of cubic and hexagonal GaN. In addition, heterocyclic Al-amides ($[Et_2AlNH_2]_3$) [14] and Al-imides ($[HAlNR]_x$ R = Et, iPr) [15] have been successfully decomposed to nanocrystalline AlN at temperatures of 1000 °C and higher under a steady flow of ammonia. In contrast, pyrolysis under Ar or N_2 yielded materials with high carbon levels. NH_3 was not only found to enhance the decomposition pathway toward a more complete alkane elimination and, as a consequence, to lower the C content of the resulting material but also to significantly increase the decomposition rate of $[Et_2AlNH_2]_3$.

Herein we report on the results obtained from ammonolysis reactions of the base-stabilized trisaminoalane Me_3N–$Al[N(H)Dipp]_3$ **I** (Dipp = 2,6-iPr$_2$–C_6H_3) in liquid ammonia and from pyrolysis studies of the resulting oligomeric compounds in a steam of NH_3. Different analytical techniques were used to monitor the progress of the reactions, including thermal analysis, solid-state NMR and powder X-ray diffraction (XRD). Since our interpretation of the ^{15}N NMR spectra relies on quantum mechanical predictions of isotropic chemical shift values, we present a set of benchmark calculations and experimental data of compounds similar to **I** in the Supporting Information.[1]

___
[1]Electronic Supplementary Information (ESI) available.

2. Experimental

All manipulations were performed by standard Schlenk techniques under an Ar-atmosphere. Solvents were freshly distilled from sodium benzophenone ketyl or Na/K-alloy and NH_3 was dried over KOH prior to use. Me_3N–$Al[N(H)Dipp]_3$ **I** was synthesized by literature method [16], [15]NH_3 was commercially available from Aldrich. MAS-NMR experiments (^{27}Al, ^{15}N) were carried out on a Varian Infinity + spectrometer equipped with a commercial 4 mm T3 MAS triple-resonance probe. The magnetic field strength was 9.4 T. Both ^{15}N and ^{27}Al spectra were acquired using continuous wave decoupling with a field strength of 100 kHz. The given chemical shift values refer to CH_3NO_2 (^{15}N) and a 1.1 M solution of $Al(NO_3)_3$ (^{27}Al) as chemical shift standards. ^{15}N NMR spectra were acquired with a ramped $^{15}N\{^1H\}$ cross-polarization experiment for the ammonolysis products and/or single-pulse excitation for some of the pyrolysis products. The spectra typically are the average of a few thousand transients acquired with a repetition delay of 1–3 s and a rotor spinning frequency of 10 kHz.

XRD-patterns of the materials were recorded on a Philips PW1050 diffractometer using Cu $K\alpha$ radiation with an AFM secondary monochromator. The materials were also characterized by means of transmission electron microscopy (TEM) using a Philips CM30ST (LaB$_6$-cathode) at 300 keV equipped with a parallel electron energy loss (EEL) spectrometer (Gatan P666) or a Philips CM300UT (FEG) at 297 keV equipped with a $2k \times 2k$ SlowScan-CCD (Gatan MSC) and an imaging filter (Gatan GIF200) for recording EEL-spectra and energy-filtered images with a second $1k \times 1k$ CCD at the end of the filter. A HP-Ge EDX-detector (Noran Voyager) was present on both transmission electron microscopes for EDX-analysis. C–K, N–K, O–K and Al–K lines were used for quantification of the EEL-data. The samples were prepared on perforated carbon foils without further grinding.

2.1. Ammonolysis studies

A solution of 3.07 g (5.0 mmol) finely powdered Me_3N–$Al[N(H)Dipp]_3$ **I** in 30 mL of liquid NH_3 and 30 mL of n-hexane was heated to reflux at −38 °C for the desired time, followed by a 2 h NH_3 boil-off. The resulting white slurry was filtered and washed two times with 20 mL of n-hexane, yielding a colorless powdery material that was evacuated overnight.

2.2. Pyrolysis studies

Materials obtained after ammonolysis of **I** for 12 h (**IIc**) were used in pyrolysis experiments. Pyrolysis experiments under a steam of N_2 and Ar yielded carbon-containing black products. Therefore, pyrolysis experiments were performed in a quartz boat under a steady steam of ammonia at 600, 800, 900, 1000 and 1150 °C, respectively.

The precursor was typically preheated at 200 °C (1 h), ramped (15 min) to the desired temperature, and held for 3 h. Light gray (600 °C) and white powders (800, 900, 1000, 1150 °C) were formed, which were analyzed by X-ray powder diffraction (XRD), ^{15}N and ^{27}Al NMR spectroscopy. In addition, the sample obtained at 1150 °C was also characterized by TEM and EEL spectroscopy.

2.3. Computational details

All calculations were performed using modules of the program package turbomole [17]. Geometries were optimized at the DFT level of theory employing the local BP86 functional [18–22] and using the valence triple zeta basis set with polarization functions on all atoms (TZVP) from the turbomole library [23]. Calculations were sped up by applying the RI approximation for computation of electronic Coulomb interactions [24].

NMR chemical shifts were calculated at the coupled-perturbed Hartree–Fock level of theory using the modules dscf and mpshift of the turbomole package [25,26] and employing the TZP basis set from the turbomole library [27]. The choice of the method was governed by the rather large size of the systems which made the application of higher-level methods like MP2 for the calculation of the chemical shifts intractable. Experience with chemical shift calculations on boron and silicon nitrides has shown, however, that already at the Hartree-Fock level good results may be obtained [28]. On the other hand it is also well known that there are cases where electron correlation plays a decisive role and the Hartree–Fock method badly fails [29].

In the framework of our approach the components of the chemical shielding tensor $\boldsymbol{\sigma}_A$ of an atom A are given by the mixed second derivative of the total energy E with respect to the nuclear magnetic moment $\boldsymbol{\mu}_A$ of atom A and the external magnetic field $\mathbf{B}$ (α and β refer to cartesian coordinates).

$$\sigma_{A\alpha\beta} = \left[\frac{\partial^2 E}{\partial \mu_{A\alpha} \partial B_\beta}\right].$$

Before the calculated values of the isotropic chemical shielding

$$\sigma_{A,\text{iso}} = \frac{1}{3}\left(\sigma_{xx} + \sigma_{yy} + \sigma_{zz}\right)$$

can be compared with experimental data, they have to be converted to the chemical shift scale. To this end the computed shielding $\sigma_{\text{ref,calc}}$ of a reference substance is related to its experimental chemical shift $\delta_{\text{ref,exp}}$ according to the following equation:

$$\delta_{\text{sample,calc}} = \delta_{\text{ref,exp}} + \sigma_{\text{ref,calc}} - \sigma_{\text{sample,calc}}$$

with the indices denoting a calculated (calc) or experimental (exp) value, the substance of interest (sample) and a reference substance (ref). The reference substance used in our calculations was the ammonium cation NH_4^+. To transfer the calculated chemical shifts to the CH_3NO_2 standard, the experimental value $\delta_{\text{ref,exp}}$ of a saturated aqueous solution of NH_4Cl was used which was experimentally determined to be -353 ppm [30].

3. Results and discussion

Reaction of three equivalents of $DippNH_2$ and $H_3Al–NMe_3$ yielded the base-stabilized trisaminoalane $Me_3N–Al[N(H)Dipp]_3$ **I**, which was obtained as colorless crystalline solid after crystallization at -10 °C [16]. **I** has been previously characterized in detail by mass and (solution) NMR spectroscopy (^1H, ^{13}C) as well as by single crystal XRD. In order to examine structural changes resulting from ammonolysis and thermolysis reactions, we characterized **I** by solid state ^{15}N NMR spectroscopy. The ^{15}N-CP-NMR spectrum of **I** shows a sharp peak at -355.1 ppm due to the coordinating NMe_3 group and a broad signal due to the amino substituents (N(H)Dipp) at -326.2 ppm, respectively. The broadening is probably caused by quadrupolar-dipolar cross terms to coordinated ^{27}Al-atoms.

3.1. Ammonolysis studies

$Me_3N–Al[N(H)Dipp]_3$ **I** was dissolved in *n*-hexane and ammonolyzed in boiling $^{15}NH_3$ at -38 °C for different times (3 h **IIa**, 6 h **IIb**, 12 h **IIc**, 48 h **IId**). Thereafter, NH_3 was allowed to boil off at -10 °C, yielding a white suspension, from which colorless crystalline solids were isolated by filtration [31]. XRD diagrams of these solids did not show any distinguished peaks indicating the complete transformation of the crystalline starting material **I** (black curve Figs. 1 and 2) into amorphous materials (red curve) under these specific reaction conditions [32].

TGA studies of as-prepared solid materials were performed in a steam of Ar. The observed mass loss was found to steadily decrease with increasing ammonolysis time (85% (3 h), 61% (6 h), 37% (12 h), 25% (48 h)), clearly demonstrating a strong relationship between the degree of
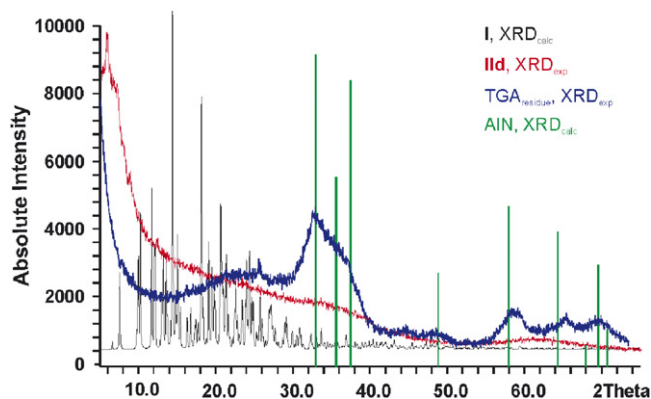

Fig. 1. XRD patterns of precursor **I** (black; calculated from single crystal X-ray data), ammonolyzed sample **IId** (red), TGA residue (blue) and of crystalline AlN (green, JCPDS 25-1133).

transamination of Me_3N–$Al[N(H)Dipp]_3$ and reaction time.

The mass loss observed for each sample starts at $100\,°C$ and is finished at about $500\,°C$. The calculated mass loss for the transformation of Me_3N–$Al[N(H)Dipp]_3$ into AlN is 93.3%. Assuming that ammonolysis of Me_3N–$Al[N(H)$-$Dipp]_3$ yields the completely transaminated oligomeric aluminum-amide-imide $[Al(NH)NH_2]_x$, the expected mass loss for the formation of AlN is 29.4%. According to this rough calculation and the experimental TGA results, Me_3N–$Al[N(H)Dipp]_3$ has to be ammonolyzed for at least 20 h to form a polymeric material, most likely $[Al(NH)NH_2]_x$, that is transaminated to a considerable extent, whereas shorter ammonolysis reactions yield polymeric materials, which still contain organic groups (NHDipp) to some extent. Obviously, the sterically

demanding organic substituents (Dipp) kinetically stabilize the trisaminoalane and hence significantly reduce its reactivity toward transamination reactions. Wells et al. [11] reported on the transamination reaction of the sterically less protected trisaminoalane $Al(NMe_2)_3$ in liquid NH_3, yielding $[Al(NH)NH_2]_x$ after 10 h [33]. XRD spectra of the black residues of the TGA studies showed very broad reflexes due to the formation of 2H-wurtzite-type AlN as shown in Fig. 1 (blue curve).

Solid state $^{15}N\{^1H\}$ CP MAS NMR spectra of the oligomeric material were recorded in order to qualitatively monitor structural changes under ammonolysis conditions (see Fig. 3). These NMR spectra show very broad peaks around $-350\,ppm$ with large half widths indicating the formation of amorphous oligomeric species featuring N atoms in different chemical environments. Even if the sample is ammonolyzed for a long time no intermediate crystalline phases containing hydrogen and nitrogen are formed.
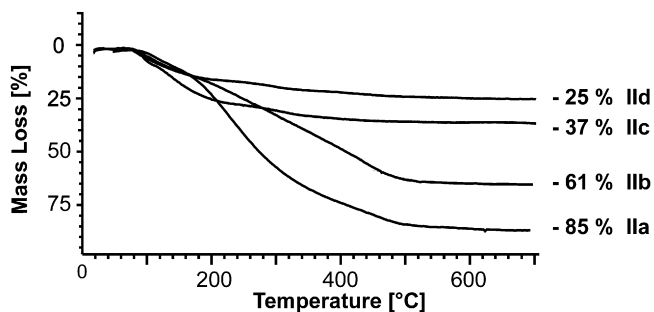
3.2. Computational studies

A series of quantum chemical computations of ^{15}N chemical shifts of several amino- and iminoalanes with bulky NHDipp substituents were performed in order to gain insight into NMR chemical shifts in chemical environments present in these molecular compounds. This should help to understand structural changes that occur under ammonolysis conditions as indicated in the ^{15}N
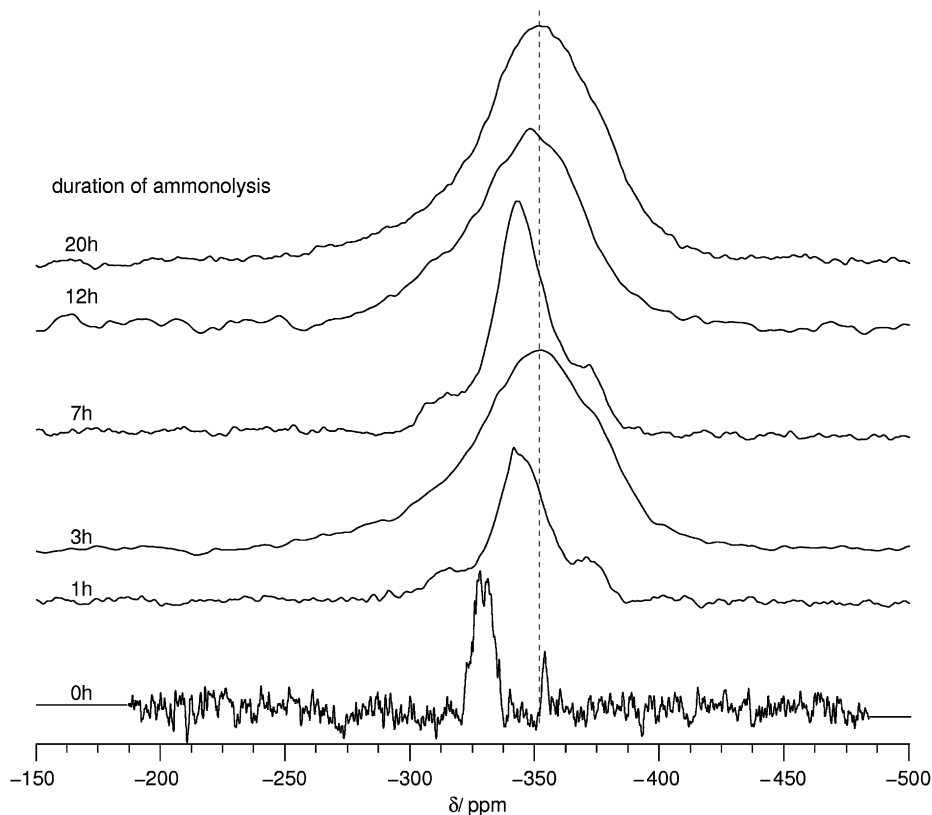

Fig. 2. TGA curves of ammonolyzed samples (black: 3 h, green: 6 h, blue: 12 h, red; 48 h).

Fig. 3. $^{15}N\{^1H\}$ CP MAS NMR spectra of the starting compound Me_3N–$Al[N(H)Dipp]_3$ and ammonolyzed samples (1, 3, 7, 12, 20 h).
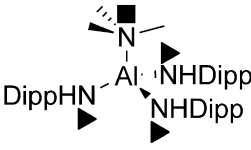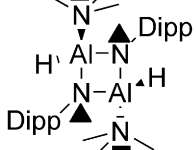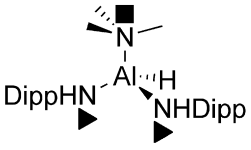
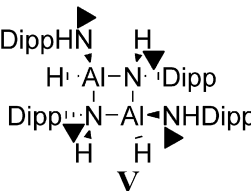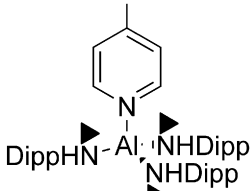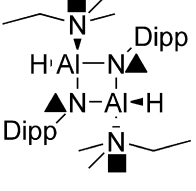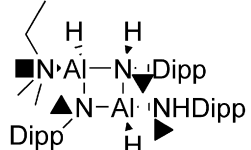|		
I	**III**	**IV**
$N(CH_3)_3$ −347 ■ $NHAlC_{ar}$ −320 ▶	$N(CH_3)_3$ −349 ■ NAl_2C_{ar} −311[1]/−312[2] ▲	$N(CH_3)_3$ −349 ■ $NHAlC_{ar}$ −314, −315 ▶
V	**VI**	**VII**
$NHAl_2C_{ar}$ −318, −319 ▼ $NHAlC_{ar}$ −313, −316 ▶	$NHAlC_{ar}$ −315...−320 ▶ NR_2C_{arom} −312 ●	$N(CH_3)_2C_2H_5$ −338[1]/ −339,−343[2] ■ NAl_2C_{ar} −307[1]/−311[2] ▲
	VIII	
	$N(CH_3)_2C_2H_5$ −339[1]/−338[2] ■ $NHAlC_{ar}$ −309[1]/−312[2] ▶ $NHAl_2C_{ar}$ −320[1]/−318[2] ▼ NAl_2C_{ar} −311[1]/−304[2] ▲	

Fig. 4. ^{15}N chemical shifts in amino- and iminoalanes containing bulky NHDipp substituents. Chemical environments are classified using different symbols. NR_3 coordinated to Al (■); NHC_{ar} bonded to Al and coordinating to another Al (▼); NHC_{ar} bonded to Al (▶); NC_{ar} bonded to two Al (▲); N bonded to two aliphatic and one aromatic C atoms (●). (1) Diagonal ligands cis and (2) diagonal ligands trans.

NMR spectra and to interpret the NMR spectra of the early stages of the transformation of the molecular precursor **I**. More detailed information about the validation of the methods for calculating chemical shifts is provided as supporting information.

Whenever available (compounds **I**, **IV** and **V**), experimentally determined crystal structures served as starting points of the geometry optimizations. Conformational differences between the optimized structures and the crystal structures were only small. Errors of calculated bond lengths of covalent Al–N bonds are only 2–3%, whereas errors of up to 5% were found for Al–N donor–acceptor bond distances. The latter finding is in accord with earlier observations that the bond strengths of dative bonds are typically underestimated by density functional theory [34]. The calculated ^{15}N NMR chemical shifts and the structures of the molecular compounds are displayed in Fig. 4.

Symbols are used for classification of different chemical environments. Taking into account the computational uncertainties of the results, it is difficult to distinguish between nitrogen atoms bonded to one phenyl group (R) and to one or two Al atoms and/or H. Clearly separated from these shifts and appearing at higher ppm values are the ^{15}N chemical shifts in NR_3Al environments.

Thereafter, we performed theoretical calculations on hydrogen-saturated clusters of crystalline AlN in order to derive a correlation between the ^{15}N chemical shift and the number of H atoms in chemical environments of the general type $NAl_{4-x}H_x$. Since the details of these calculations are beyond the scope of this paper [35], only a rough description is given here. Clusters of different sizes were generated starting from cut-offs of crystalline wurtzite and zinc-blende AlN. Dangling bonds on the surfaces were saturated by hydrogen atoms. It turned out that it is
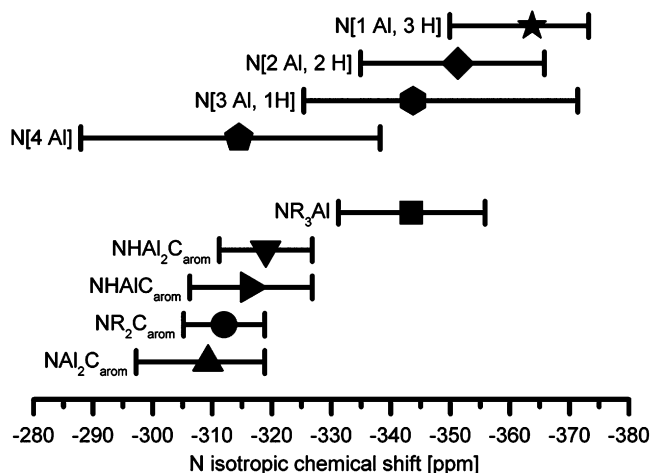
Fig. 5. ^{15}N chemical shifts in different chemical environments of amino- and iminoalanes (lower part of the diagram) and in $NAl_{4-x}H_x$ environments of AlN clusters (upper part of the diagram). The symbols mark the mean values of the chemical shifts, bars denote the range of the chemical shifts plus an uncertainty of the calculated data of 6.8 ppm.

necessary to carefully choose the number of electrons of the clusters. This was achieved in the following way: H atoms in positions of coordinative-bonded N atoms contributed two electrons, H atoms in positions of coordinative-bonded Al atoms contributed no electron, and all other H atoms contributed one electron. This scheme consequently resulted in the formation of charged clusters. The charges were kept as small as possible by suitable choice of the cluster shape. The positive or negative charges of all clusters did not exceed ± 3. Calculation of the chemical shifts of the central atoms of the largest clusters confirmed that the electronic structure resembles that of solid AlN. The structures of all clusters were optimized under symmetry restrictions (C_{3v} for wurtzite AlN clusters and T_d for zinc-blende AlN clusters). For obtaining trends of the chemical shifts we examined all nitrogen atoms of these clusters. With decreasing number of H atoms bonded to the N atom, δ was found to be shifted to higher (less negative) ppm values. Fig. 5 gives an overview of all calculated N chemical shifts [36]. The symbols used for
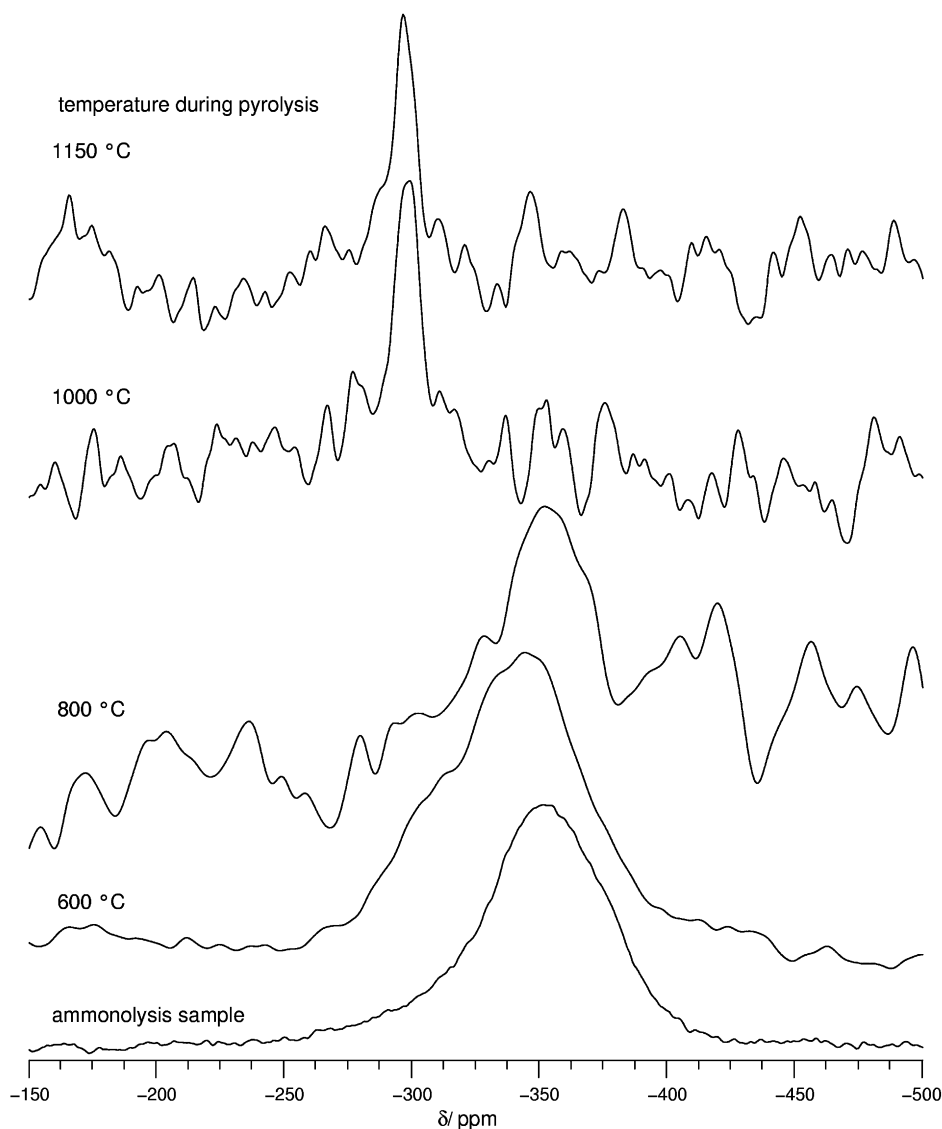

Fig. 6. ^{15}N MAS NMR spectra of samples pyrolyzed for 5 h in a stream of NH$_3$ at the given temperatures; the samples pyrolyzed above 800 °C were acquired with a Hahn-echo since only the samples pyrolyzed at 600 and 800 °C showed a cross-polarization ^{15}N{^{1}H} signal.

classification of different chemical environments are the same as in Fig. 4.

The computational results allow a qualitative interpretation of the broad ^{15}N NMR signals recorded at different stages of the ammonolysis reaction. The broad shoulder at high ppm values (left side of the peak), which can be ascribed to the presence of NAl$_2$C, NHAlC and NHAl$_2$C units in the samples, decreases with increasing ammonolysis time whereas the shoulder at low ppm values (right side of the peak), which can be attributed to the formation of NAlH$_3$ and NAl$_2$H$_2$ moieties, increases in intensity. Even though an exact differentiation of the different NAl$_2$(R,H)$_{1,2}$ environments solely based on the ^{15}N NMR data is not possible since their calculated chemical shifts fall into roughly the same range, the data strongly indicate ongoing substitution reactions of the starting NHDipp and NMe$_3$ groups by NH$_2$ and NH$_3$ groups (transamination reaction) with increasing ammonolysis time. These findings also perfectly agree with the results obtained from TGA/DTA studies.

3.3. Thermolysis studies

Oligomeric material obtained from ammonolysis reactions of Me$_3$N–Al[N(H)Dipp]$_3$ for 12 h (**IIc**) were pyrolyzed for 5 h at 600 and 800 °C, respectively, in an Ar flow. Black, amorphous solids were obtained in both cases, which did not show any distinguished reflexes in XRD experiments. The black color indicates the presence of sufficient amounts of carbon in the materials, which was verified by EEL spectroscopy [37]. The formation of carbon-contaminated AlN has been previously observed in pyrolysis reactions of *single source precursors* such as [HAl^{i}Pr]$_6$ and [R$_2$AlNH$_2$]$_3$ (R = Me, Et), respectively, in a steady flow of N$_2$ or Ar. Since the addition of NH$_3$ is known to enhance the quality of the resulting AlN by significant reduction of the carbon content, to increase the rate of decomposition and to improve the crystallinity of the resulting materials [14], we investigated the pyrolysis of **IIc** in a steady steam of NH$_3$. Samples of **IIc** were pyrolyzed at 500, 800, 1000 and 1150 °C for 5 h, yielding colorless materials.

^{15}N MAS NMR spectra of the resulting materials significantly change with increasing pyrolysis temperature. Owing to the low NMR sensitivity of the isotope ^{15}N, the spectra were recorded in a non-quantitative manner. The materials formed at 600 and 800 °C show a broad peak at about −350 ppm as was observed for the ammonolyzed material (Fig. 6). However, the center is shifted to the left side to higher ppm values. In remarkable contrast, samples pyrolyzed at 1000 and 1150 °C show strong sharp resonances at −299 and −296 ppm, respectively. These correspond very well with the ^{15}N chemical shift observed for crystalline AlN (−295 ppm) as determined by a ^{15}N{^{27}Al} FAM-CP-MAS experiment [38,43]. Small differences in the chemical shifts can be explained by susceptibility changes of the surrounding matrix. Obviously,
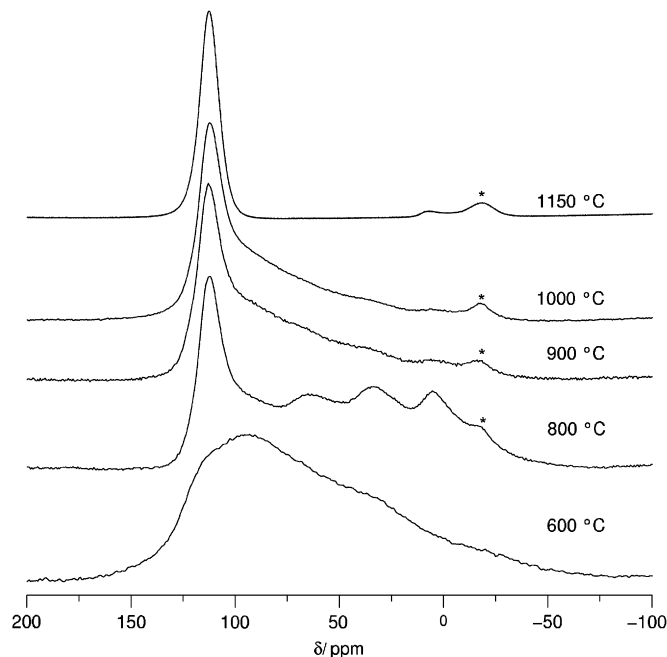

Fig. 7. Central part of ^{27}Al MAS NMR spectra of samples pyrolyzed for 5 h in a stream of NH$_3$ at the given temperatures; asterisks mark rotational sidebands.

crystalline AlN grows out of the amorphous polymeric AlN matrix at temperatures higher than 1000 °C.

^{27}Al MAS NMR spectra also show significant changes (Fig. 7). The spectrum of the material obtained at 600 °C shows a very broad resonance at 90 ppm, whereas the materials pyrolyzed at 800 and 900 °C show very sharp resonances at 111 ppm and some distinguished peaks at higher field (63, 32, 4 ppm, 800 °C sample) or a broad shoulder at the left side of the main signal (900 °C). In sharp contrast, samples formed at 1000 and 1150 °C only show sharp single resonances at 112 and 113 ppm, respectively, which also agree very well with the ^{27}Al resonance of crystalline AlN (112.7 ppm).

XRD powder patterns clearly demonstrate the formation of crystalline AlN at pyrolysis temperatures above 1000 °C (Figs. 8 and 9). Patterns of the materials formed below 1000 °C did not show any distinguished peaks proving the resulting material to be amorphous. In contrast, the material obtained at 1150 °C gave sharp reflexes in the XRD, clearly revealing the formation of crystalline 2H-wurtzite-type AlN.

TEM investigations on the crystalline AlN obtained at 1150 °C showed agglomerates of plate-like thin crystals with an average diameter of the crystallites of 10 nm. The crystals are randomly distributed and show no preferred orientation. Selected area electron diffraction (SAED) yielded Debye–Scherrer ring patterns, which could be simulated with wurtzite-type AlN (Fig. 8c) [39]. The lattice parameters obtained from these patterns (a: 310(2); c: 499(3) pm) agree perfectly with literature data [40]. It is hardly possible to bring the nanocrystals in distinguished zone axis orientation. Crystals lying close to zone axis

conditions by chance showed distances of the lattice fringes of AlN. The AlN nanocrystals are covered by a small amorphous seam. EEL-spectra of the material clearly revealed the presence of aluminum and nitrogen as well as small traces of oxygen and silicon. Si contamination occurs from the use of joint grease during the ammonolysis and pyrolysis experiments. There is no carbon detectable in

sample regions overhanging holes of the underlying carbon films. The N/O-ratio determined by quantification of the EEL-spectra decreases with decreasing thickness of the transmitted area. The thickness was determined from the ratio of in-elastically scattered electrons to elastically scattered electrons. Thus, the amount of oxygen is caused by a surface layer and the thicker the sample, the lesser the amount of oxygen relatively to the nitrogen concentration. The ELNES fingerprint of the N–K edge compares well with literature values as found in the EEL and X-ray database [41]. In addition, they are in good agreement with values assigned to non-oxidized AlN as reported by McKenzie and Craven [42].

Fig. 8. Calculated and experimental powder X-ray diffraction pattern of crystalline AlN obtained at 1150.

4. Conclusions

Ammonolysis of $Me_3N–Al[N(H)Dipp)]_3$ yielded amorphous, oligomeric materials, which can be pyrolyzed under a steady flow of NH_3 to give pure AlN. Theoretical calculations were performed in order to identify potential reaction intermediates. Solid-state NMR spectroscopy (^{15}N, ^{27}Al) and XRD studies clearly demonstrated the formation of crystalline AlN at temperatures higher than $1000\,^{\circ}C$.
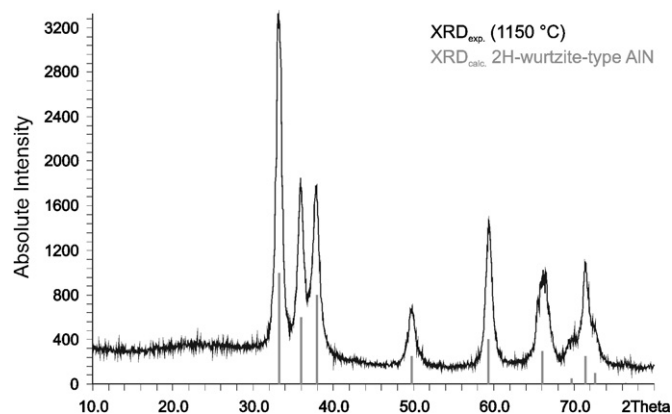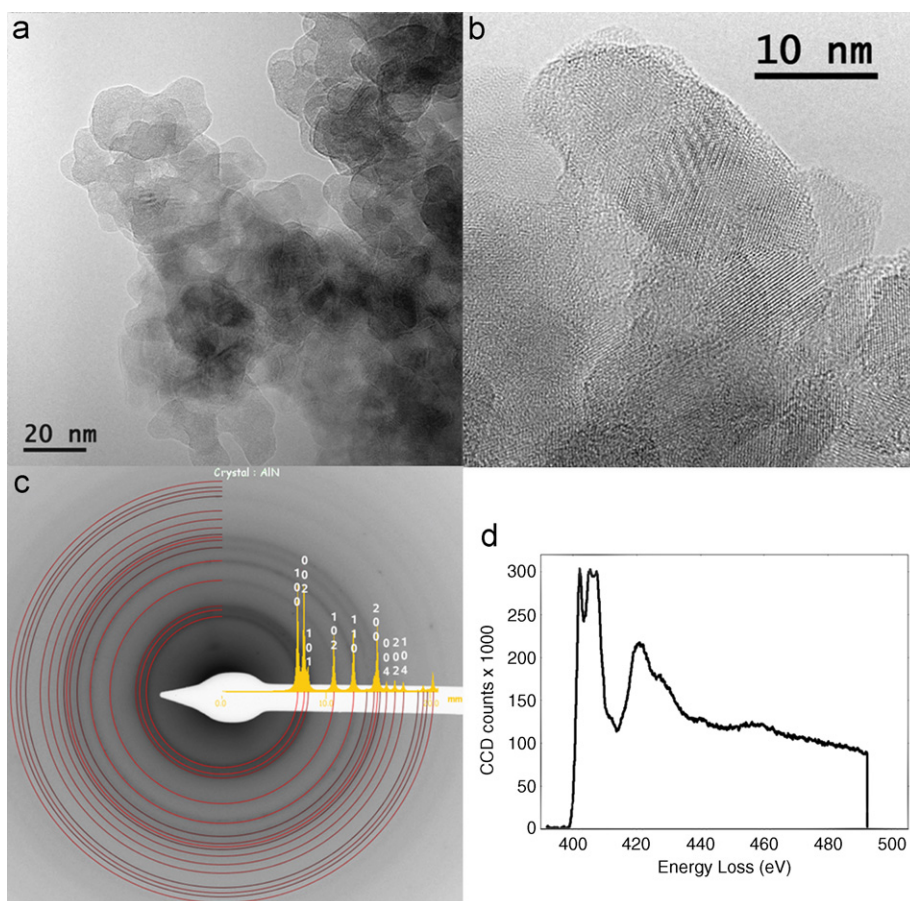

Fig. 9. TEM bright field images of crystalline AlN nanoparticles obtained at 1150 °C (a, b). Electron diffraction pattern of AlN and simulation (c) and ELNES of the N–K edge (d).

Appendix A. Supporting Information

Supplementary data associated with this article can be found in the online version at doi:10.1016/j.jssc.2007.12.026.

References

[1] D. Rühelä, M. Ritala, R. Matero, M. Leskelä, J. Jokinen, P. Haussalo, Chem. Vap. Deposition 2 (1996) 277.
[2] Y. Qui, L. Gao, J. Eur. Ceram. Soc. 23 (2003) 2015;
E. Kroke, L. Löffler, F.F. Lange, R. Riedel, J. Am. Chem. Soc. 85 (2002) 3117.
[3] T. Suehiro, J. Tatami, T. Meguro, S. Matsuo, K.J. Komeya, Eur. Ceram. Soc. 22 (2002) 521.
[4] R. Fu, K. Chen, X. Xu, J.M.F. Ferreira, Mater. Lett. 59 (2005) 2605.
[5] M. Pouget, J.P. Lecompte, J. Eur. Ceram. Soc. 16 (1996) 521.
[6] See the following and references cited therein: K. Sardar, C.N.R. Rao, Solid State Sci. 7 (2005) 217.
[7] For review articles see: A.C. Jones, S.A. Rushworth, J. Auld, J. Cryst. Growth 146 (1995) 503;
A.C. Jones, Chem. Soc. Rev. (1997) 101;
A.V. Timoshkin, H.F. Schaefer III, Chem. Rec. 2 (2002) 319.
[8] L. Baixia, L. Yinkui, L. Yi, J. Mater. Chem. 3 (1993) 117.
[9] E. Wiberg, A. May, Z. Naturforsch. B 10 (1955) 229.
[10] E. Wiberg, A. May, Z. Naturforsch. B 10 (1955) 231.
[11] J.F. Janik, R.L. Wells, J.L. Coffer, J.V. St. John, W.T. Pennington, G.L. Schimek, Chem. Mater. 10 (1998) 1613.
[12] J.F. Janik, R.L. Wells, Chem. Mater. 8 (1996) 2708.
[13] J.-W. Hwang, J.P. Campbell, J. Kozubowski, S.A. Hanson, J.F. Evans, W.L. Gladfelter, Chem. Mater. 7 (1995) 517.
[14] F.C. Sauls, W.J. Hurley, L.V. Interrante, P.S. Marchetti, G.E. Maciel, Chem. Mater. 7 (1995) 1361.
[15] Y. Sugahara, T. Onuma, O. Tanegashima, K. Kuroda, C. Kato, J. Ceram. Soc. Jpn. 100 (1992) 101;
Y. Saito, S. Koyama, Y. Sugahara, K. Kuroda, J. Ceram. Soc. Jpn. 104 (1996) 143;
S. Koyama, H. Takeda, Y. Saito, Y. Sugahara, K. Kuroda, J. Mater. Chem. 6 (1996) 1055;
Y. Sugahara, S. Koyama, K. Kuroda, Key Eng. Mater. 159,160 (1999) 77.
[16] T. Bauer, S. Schulz, H. Hupfer, M. Nieger, Organometallics 21 (2002) 2931.
[17] R. Ahlrichs, M. Bär, H.-P. Baron, R. Bauernschmitt, S. Böcker, P. Deglmann, M. Ehrig, K. Eichkorn, S. Elliot, F. Furche, F. Haase, M. Häser, C. Hättig, H. Horn, C. Huber, U. Huniar, M. Kattannek, A. Köhn, C. Kölmel, M. Kollwitz, K. May, C. Ochsenfeld, H. Öhm, A. Schäfer, U. Schneider, M. Sierka, O. Treutler, B. Unterreiner, M. von Arnim, F. Weigend, P. Weis, H. Weiss, Turbomole (vers. 5–6), 2002.
[18] P.A.M. Dirac, Proc. Roy. Soc. A 123 (1929) 714.
[19] J.C. Slater, Phys. Rev. 81 (1951) 385.
[20] S. Vosko, L. Wilk, M. Nusair, Can. J. Phys. 58 (1980) 1200.
[21] A.D. Becke, Phys. Rev. A 38 (1988) 3098.
[22] J.P. Perdew, Phys. Rev. B 33 (1986) 8822.
[23] A. Schäfer, C. Huber, R. Ahlrichs, J. Chem. Phys. 100 (1994) 5829.
[24] K. Eichkorn, F. Weigend, O. Treutler, R. Ahlrichs, Theor. Chem. Acc. 97 (1997) 119.
[25] M. Häser, R. Ahlrichs, J. Comp. Chem. 10 (1989) 104.
[26] M. Häser, R. Ahlrichs, H.-P. Baron, P. Weis, H. Horn, Theor. Chim. Acta 83 (1992) 455.
[27] A. Schäfer, H. Horn, R. Ahlrichs, J. Chem. Phys. 97 (1992) 2571.
[28] M. Doerr, C.M. Marian, Sol. State Nucl. Magn. Reson. 30 (2006) 16;
C.M. Marian, M. Gastreich, Sol. State Nucl. Magn. Reson. 19 (2001) 29.
[29] J. Gauss, J.F. Stanton, Adv. Chem. Phys. 123 (2002) 355.
[30] M. Witanowski, L. Stefaniak, S. Szymanski, H. Januszewski, J. Magn. Reson. 28 (1977) 217.
[31] The filtrate gave an oily residue after evaporation of the solvent, which was shown by ^1H NMR spectroscopy to consist of DippNH$_2$, clearly demonstrating the occurrence of transamination reactions.
[32] The powder X-ray diffraction pattern of I was calculated from the single crystal X-ray data.
[33] The overall reaction time reported for the reaction of Al(NMe$_2$)$_3$ in liquid NH$_3$ was 8 h, followed by a 2 h NH$_3$ boil-off. The calculated weight loss for [Al(NH)NH$_2$]$_x$ is 29.4%, but the TGA curve showed a mass loss of only 20%.
[34] S. Reinhardt, C.M. Marian, I. Frank, Angew. Chem. Int. Ed. Engl. 133 (2001) 3795;
R. Ahlrichs, F. Furche, S. Grimme, Chem. Phys. Lett. 325 (2000) 317.
[35] The details will be presented in a separate publication: M. Doerr, C.M. Marian, Solid State NMR, in preparation. At present they are available as part of a PhD thesis: Doerr, M. PhD thesis, University of Düsseldorf 2006. URL: ⟨http://docserv.uni-duesseldorf.de/servlets/DocumentServlet?id = 3461⟩.
[36] Note that the ranges of the chemical shifts are based on different numbers of data points, which explains the different widths of the shift intervals in Fig 5. The largest number of data points (37) was available for the chemical shifts in NAl$_4$ environments. Smaller numbers of data points were available for chemical shifts in environments NAl$_{4-x}$H$_x$ with larger numbers of H atoms because such environments are only found at the surfaces of the clusters. The interval of the chemical shifts in NAlH$_3$ environments based on only four data points.
[37] EEL spectroscopy studies clearly revealed the presence of carbon in the material.
[38] P.K. Madhu, A. Goldbourt, L. Frydman, S. Vega, Chem. Phys. Lett. 307 (1999) 41.
[39] P. Stadelman, Jems Electron Microscopy Software, EPFL Lausanne, Switzerland, 1999–2007.
[40] PDF2 file #025-1133 JCPDS-International Centre for Diffraction Data, USA.
[41] EELS and X-ray Database. ⟨http://www.cemes.fr/~eelsdb⟩.
[42] M. MacKenzie, A.J. Craven, J. Phys. D: Appl. Phys. 33 (2000) 1647. More detailed EELS data are supplied with the supplement material.
[43] M. Eden, J. Grins, Z. Shen, Z. Weng, J. Magn. Reson. 169 (2004) 279.